# Simulating tornado-like flows

Gillmeier, Steffi; Sterling, Mark; Hemida, Hassan

*Document Version*
Peer reviewed version

[Link to publication on Research at Birmingham portal](Link to publication on Research at Birmingham portal)

# Simulating Tornado-Like Flows – the Effect of the Simulator's Geometry

S. Gillmeier[1], M. Sterling[2], H. Hemida[3]

*Department of Civil Engineering, School of Engineering, University of Birmingham, Edgbaston, Birmingham, B15 2TT, United Kingdom,*
*[1]stefaniegillmeier-wls@web.de, +31 402472414*
*[2]m.sterling@bham.ac.uk, [3]h.hemida@bham.ac.uk*

**ABSTRACT**

*Within the wind engineering community, a series of physical simulators of differing geometries have been used to investigate the flow-field of tornado-like vortices. This paper examines the influence that the geometry of a simulator can have on the generated flow field. Surface pressure and velocity data have been measured for two swirl ratios (S = 0.30 and S = 0.69) in two different simulators of different scale and varying geometry. The results of this research suggest that far from being a mature research field, there are still many unresolved questions that need to be addressed before data obtained from such simulators can be used with confidence in practice.*

Keywords: Tornado-like vortex; Physical simulation; Simulator's design, Geometric parameters; Aspect ratio; Swirl ratio

## 1. INTRODUCTION

In recent years, increasing attention has been paid to the effects of non-stationary, non-synoptic winds with downbursts [1 - 3] and in particular tornadoes generating much significant research [4]. The latter is perhaps not too surprising when one considers the impact of such winds. For example, in 2011 North America experienced one of the most destructive tornado seasons with approximately 1600 tornado outbreaks reported and the total damage exceeding \$28bn [5]. Considerable tornado losses also occur elsewhere around the world but not necessarily as frequently or to such an extent. The transient and violent nature of such events ensures that obtaining full-scale data at a resolution of interest to wind engineers is fraught with challenges. However, a number of excellent full-scale datasets have been obtained despite the aforementioned difficulties [6 – 14]. Unfortunately, the expense of obtaining such data and the spatial resolution of the flow field, i.e., at heights considerably larger than average low-rise buildings, prevent their general adoption in the wind engineering community, although this is slowly changing [15]. As a result, recourse is often made to physical and numerical simulations, with the former typically preceding the latter.

Hence, a variety of large (> 10m in diameter), medium (~ 2m-5m) and small (< 1m) scale physical simulators purporting to generate tornado-like flow fields have been used to investigate a variety of tornado related issues [16 - 24]. The vast majority of these simulators embody the principles initially developed by Ward [16], i.e., a tornado-like wind is created by generating a circulation in the presence of a suction updraft. Surprisingly, relatively little has been reported concerning the geometry of such simulators, with most new simulators having a large degree of geometric similarity.

48    Davies-Jones [25] undertook a simple dimensional analysis of a Ward-type simulator and
49    highlighted six non-dimensional parameters of potential importance. The following four define the
50    geometry of the simulator:
51
$$2H_1/D_3 \equiv G_a \tag{1}$$
52
53
$$H_2/D_1 \equiv G_b \tag{2}$$
54
55
$$D_2/D_1 \equiv G_c \tag{3}$$
56
57
$$D_3/D_1 \equiv G_d \tag{4}$$
58
59
60    where $H_1$ and $D_3$ are the height of the convergence chamber and the diameter of the updraft hole,
61    respectively. $H_2$ and $D_1$ are the height of the convection chamber and the diameter of the
62    convergence chamber, and $D_2$ is the diameter of the convection chamber. Exact locations of the
63    aforementioned geometric variables are also illustrated in figure 1. A factor of two was introduced
64    in equation (1) because the ratio between convergence chamber height and updraft radius ($D_3/2$) is
65    frequently referred to as the aspect ratio (Eq. 1). Notwithstanding this, of the parameters listed in
66    equations (1 – 4), over the years the main geometric parameter which has tended to be kept constant
67    as new simulators were constructed is the aspect ratio (Eq. 1). Intuitively, one would expect the
68    aspect ratio to play a major role in governing the generated flow field [26]; however, whether it is
69    appropriate to elevate this parameter (Eq. 1) over the others (Eq. 2 – 4) is debatable and is
70    investigated below. It also needs to be mentioned that there are other parameters that have not been
71    taken into account, such as the design or the number of guide vanes, which could potentially affect
72    the generated vortex flow structure.
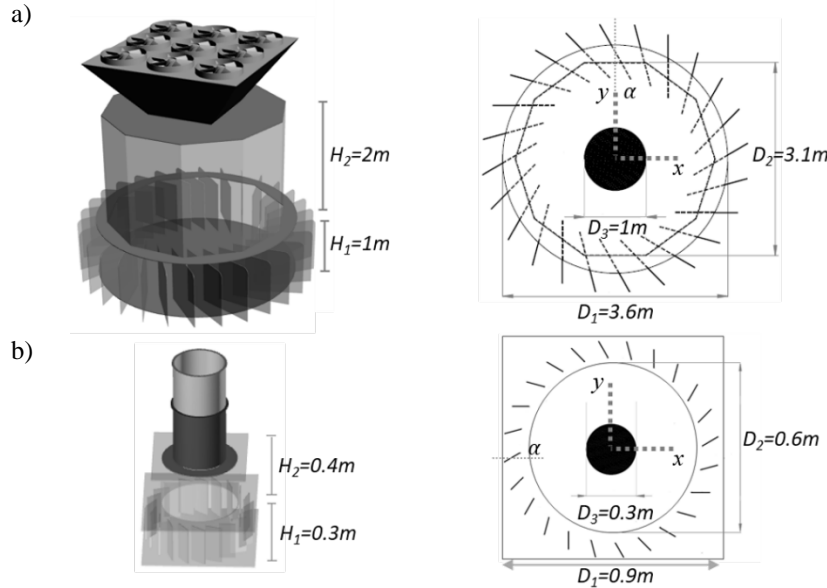73



74
75    **Fig. 1** An illustration of (a) the medium-scale (*M1*) and (b) the small-scale (*S1*) tornado-like vortex generator. $H_1$ and
76        $D_1$ show the height and diameter of the convergence chamber, $H_2$ and $D_2$ show the height and diameter of the
77                    convection chamber and $D_3$ is the diameter of the updraft hole

78   Davies-Jones [25] acknowledged that the generated flow field is not simply a function of the
79   geometric parameters but also a function of the volume flow rate through the simulator and the
80   circulation at a certain location in the simulator. As a result, two additional non-dimensional
81   parameters have received attention in the literature, i.e., the Reynolds number, *Re*, (Eq. 5) and a
82   parameter which describes the effect of rotation on the flow field - the swirl ratio, *S*, (Eq. 6).
83
84
$$Re = \frac{2Q}{vD_3} \qquad\qquad (5)$$
85
86
$$S = \frac{tan(\alpha)}{2G_a} \qquad\qquad (6)$$
87
88   where *Q* is the volume flow rate through the simulator, *v* is the kinematic viscosity of air and α is
89   the guide vane angle relative to the radial velocity component.
90
91   Equation (6) is adopted in this research since it is the version which also has been widely used in
92   Ward-type simulators and thus is helpful in undertaking relative comparisons between such
93   simulators. It is acknowledged that such a definition raises a number of challenges, not least
94   determining the equivalent full-scale value. Notwithstanding the issues that exist regarding the
95   swirl ratio definition, the swirl ratio is generally accepted as an important parameter for tornado-
96   like simulations and its effect on the generated vortex flow field has been investigated thoroughly
97   [16 - 18, 21 - 25, 27 - 30].
98
99   Using a medium-scale simulator of fixed geometry and a small-scale simulator of variable
100  geometry (Figure 1), this paper will investigate the influence of the simulators' varying geometric
101  parameters on the simulation of tornado-like vortices. Section 2 of the paper outlines the
102  experimental methodology, whereas section 3 presents results. Concluding remarks are given in
103  section 4, which state that the approach (adopted by many) of 'simply' matching the aspect ratio
104  and swirl ratio is insufficient to ensure flow field parity between vortices generated in different
105  simulators.
106
107  In keeping with the work of previous authors, the investigation contained herein focuses on the
108  behaviour of mean flow variables. However, it is acknowledged that tornadoes are non-stationary
109  phenomenon and when simulated physically, a degree of non-stationarity often attributed to vortex
110  wandering [e.g. 31] has been observed. Nevertheless, and as shown below, the importance of the
111  geometric parameters in equations (1 - 4) can be observed through examining the mean flow
112  parameters alone.
113
114  **2. EXPERIMENTAL METHODOLOGY**
115
116  **2.1. Tornado-like vortex simulators**
117
118  Figure 1 provides a schematic of the two Ward-type simulators used in the current research. The
119  medium-scale simulator (*M1*) has a total height ($H_1 + H_2$) of 3m and a convergence chamber
120  diameter of 3.6m. The small-scale simulator (*S1*) has a variable height between 0.4m – 0.7m
121  (depending on setting, i.e., $H_2$ is variable) and a convergence chamber diameter of 0.9m. In both
122  cases, angular momentum is introduced by guide vanes around the convergence chamber, which

123 can be set to different angles. By changing the guide vane angle (α), the vorticity in the flow can
124 be altered and different vortex structures can be generated. The geometric configurations of *M1*
125 and *S1* result in an aspect ratio of $G_a = 2$ (Table 1a). It is noted that the aspect ratio is relatively
126 large compared to the aspect ratios of simulators at Western University [22], Texas Tech University
127 [19, 24] and Iowa State University (18). However, the tornado simulator at Purdue University [32]
128 and the original Ward simulator [16] allow the simulation of tornado-like vortices with similar
129 aspect ratios.
130 In order to investigate whether geometric parameters defined by equation (2 – 4) influence the
131 generated tornado-like flow field, eight simulations have been undertaken (details of which are
132 given in table 1), in order to evaluate:

134 *T1)*    the effect of the simulator's geometry with constant aspect ratio and swirl ratio. In this case,
135          the aspect ratio was fixed at 2 and the medium-scale (*M1*) and small-scale simulator (*S1*)
136          were used.

138 *T2)*    the effect that the convection chamber may have on the simulation. In this case, the
139          convection chamber height ($H_2$) of the small-scale simulator was reduced from $H_2 = 0.40$m
140          (*S1*) to $H_2 = 0.25$m (*S2*) to $H_2 = 0.10$m (*S3*), whilst all other geometric lengths were kept
141          constant.

143 Geometric parameters listed in equations (1 – 4) are presented in table 1a for the medium-scale
144 (*M1*) and the small-scale simulators (*S1 – S3*). In all cases, the flow fields of two swirl ratios (*S* =
145 0.30 and *S* = 0.69) are investigated. It is noted that for this research the swirl ratio is defined based
146 on the guide vane angle (Eq. 3) but a detailed investigation regarding the swirl ratio and its
147 alternative definitions is presented in section 3.1.3. Over the small range of the Reynolds numbers
148 investigated (Table 1b), no Reynolds number dependency was found and as such is not considered
149 further.

151 Table 1: Overview of non-dimensional geometric (a) and dynamic (b) parameters for the simulations undertaken

| a) | $G_a$ | $G_b$ | $G_c$ | $G_d$ |
|---|---|---|---|---|
| *M1* | 2 | 0.56 | 0.86 | 0.28 |
| *S1* | 2 | 0.44 | 0.67 | 0.33 |
| *S2* | 2 | 0.27 | 0.67 | 0.33 |
| *S3* | 2 | 0.11 | 0.67 | 0.33 |

152

| b) | $Re \cdot 10^5$ | |
|---|---|---|
| | *S = 0.30* | *S = 0.69* |
| *M1* | 10.1 | 9.1 |
| *S1* | 2.9 | 2.4 |
| *S2* | 2.6 | 2.2 |
| *S3* | 2.7 | 2.6 |

153
154 **2.2. Normalisation**
155

156    Circumferential ($u_\theta$), radial ($u_r$) and vertical ($u_z$) velocity components are normalised by a reference
157    wind speed ($u_{ref}$) which is based on the volume flow rate ($Q$) measured across the updraft diameter
158    $D_3$ of the simulators divided by the corresponding area of the updraft. Surface pressures ($p$) of
159    corresponding simulations are normalised by the corresponding dynamic pressure ($p_{ref}$) which is
160    based on ($u_{ref}$). Radial and vertical distances are normalised by the updraft diameter ($D_3$) and the
161    convergence chamber height ($H_1$), respectively. Table 2 provides a list of relevant parameters
162    required for the normalisation of the simulations conducted in *M1*, *S1*, *S2* and *S3* for $S = 0.30$ and
163    $S = 0.69$.
164
165    Table 2: Volume flow rate, reference wind speed and reference pressure for the normalisation of results obtained in
166    *M1*, *S1*, *S2* and *S3* for $S = 0.30$ and $S = 0.69$

|  | $Q$ [$m^3/s$] | | $u_{ref} = 4Q / (\pi\ D_3^2)$ [m/s] | | $p_{ref} = \frac{1}{2}\ \rho\ u_{ref}^2$ [$Nm^{-2}$] | |
|---|---|---|---|---|---|---|
|  | *S = 0.30* | *S = 0.69* | *S = 0.30* | *S = 0.69* | *S = 0.30* | *S = 0.69* |
| *M1* | 7.6 | 6.9 | 9.6 | 8.7 | 55.3 | 45.4 |
| *S1* | 0.7 | 0.6 | 9.1 | 7.7 | 49.7 | 35.6 |
| *S2* | 0.6 | 0.5 | 8.3 | 7.1 | 41.3 | 30.2 |
| *S3* | 0.6 | 0.6 | 8.6 | 8.4 | 44.4 | 42.3 |

167
168    **2.3. Measurement setup and data quality**
169
170    The pressure data were measured on the ground plane along two mutually perpendicular lines
171    denoted as *x* and *y* (Figure 1) every 0.01s for a period of 60 seconds using a Multi-Channel-
172    Pressure-System manufactured by Solution for Research Ltd. Surface pressure taps are distributed
173    along these lines with a spacing of 0.01m and 0.05m from the simulator's centre up to a distance
174    of 0.15m and 0.75m for the small-scale simulators (*S1 – S3*) and the medium-scale simulator (*M1*),
175    respectively.
176
177    Point velocity measurements were obtained every 0.01s for a period of 80 seconds using a Cobra
178    Probe (TFI instrumentation – Series 100 Cobra Probe) which was mounted to a two-axis traverse
179    system inside the simulators. This traverse system enabled the probe to be positioned with an
180    accuracy of $\pm$1mm at nine heights (*z*) above the simulator's surface (0.01m, 0.03m, 0.05m, 0.07m,
181    0.10m, 0.13m, 0.15m, 0.17cm and 0.20m) in the small-scale simulators (*S1 – S3*) and nine heights
182    above the simulator's surface (0.01m, 0.05m, 0.10m, 0.15m, 0.20m, 0.25m, 0.30m, 0.40m, 0.50m)
183    in the medium-scale simulator (*M1*). The corresponding radial spacing of measurement positions
184    from the centre of each convergence chamber up to a distance of 0.18m (small simulator) and
185    0.60m (medium simulator) was 0.010m and 0.025m, respectively. Whilst the Cobra Probe was
186    supported by a relatively small traverse system, every effort was made to minimise its impact, with
187    the main supporting section being located at a distance greater than the corresponding convergence
188    chamber height from the measurement location. The actual size of the traverse system in *M1* and
189    *S1* was ~$10^3$ smaller than the size of the convergence chambers. However, it is acknowledged that
190    there could be an impact on the flow (similar to most systems in boundary layer wind tunnels). In
191    an attempt to quantify the potential influence of the system, a series of pressure measurements were
192    undertaken for a variety of swirl ratios with and without the system in place. No noticeable effect
193    was observed on the measured data.
194

195 In order to evaluate potential differences in the simulations, it is important to account for
196 experimental uncertainties. The experimental uncertainty is a combination of uncertainties due to
197 measuring a finite time series (statistical uncertainty), operator error such as probe and guide vane
198 angle positioning (repeatability) and the uncertainty of the measurement device itself. A detailed
199 explanation of different uncertainties for measurements conducted in *M1* can be found in Gillmeier
200 et al. [23]. A similar methodology was followed for velocity and surface pressure measurements in
201 *S1 – S3* and for the sake of clarity are briefly outlined below.
202
203 In this research, pressure transducers (*HCLA12X5DB*) with a typical uncertainty of $\pm 5$ Nm$^{-2}$ were
204 used. The Cobra Probe is accurate to within $\pm 0.5$ m/s for the velocity vector up to a turbulence
205 intensity of ~30%. Therefore, positions with a turbulence intensity greater than 30% are excluded
206 from the comparison analysis. Furthermore, the Cobra Probe can measure velocity data greater
207 than 2 m/s within a cone of influence of $\pm 45°$. These limitations can have a direct influence on the
208 measured data. For example, if the recorded data quality (defined as the percentage of velocity
209 samples of a measured time series which are greater than 2 m/s and have an angle of attack less
210 than $\pm 45°$) is less than 100%, then this can introduce a bias in the calculated velocity vector – the
211 lower the data quality the greater the potential bias. To minimize the bias in time averaged
212 velocities, only those positions with a data quality of greater than 80% were accepted for the
213 comparison analysis. This threshold is assumed to provide a suitable compromise between data
214 quality and quantity.
215
216 In order to assess the statistical uncertainty, convergence tests were conducted for 600 seconds at
217 the core radius (*R*) of corresponding simulations. (i.e., at the radial distance (*r*) and height (*z*) at
218 which the overall maximum circumferential velocity component occurs). For surface pressures,
219 convergence tests were conducted at the centre of the simulators. It was observed that after 60
220 seconds, the uncertainty in determining time-averaged surface pressures decreased to below $\pm 6\%$
221 and $\pm 1\%$ of the time-average obtained after 600 seconds in all simulations for $S = 0.30$ and $S =$
222 0.69, respectively. For velocity measurements, an averaging time of 80 seconds allows to determine
223 circumferential and vertical velocities with an uncertainty below $\pm 2\%$ for all simulations.
224 Statistical uncertainties of radial velocity components are approximately $\pm 3\%$ and $\pm 0.5\%$ for $S =$
225 0.30 and $S = 0.69$, for all simulations.
226
227 The measurement repeatability is analysed in form of a distribution of all possible differences of
228 repetition measurement datasets. Surface pressure and velocity measurements were repeated five
229 times along the radial profile at the surface and at a height of $z = 0.01$m for each swirl ratio. The
230 standard deviation ($\sigma$) of the corresponding distributions was chosen as a representative measure
231 to evaluate the repeatability (Table 3). It was found that the repeatability is swirl ratio dependent.
232 Furthermore, for $S = 0.30$ the repeatability of surface pressure measurements seems to be dependent
233 on the radial distance. For that reason, a repeatability dependent on *r* is introduced for the surface
234 pressures obtained with $S = 0.30$ since a uniform value would highly underestimate the repeatability
235 of measurement positions close to the vortex centre, and highly overestimate the repeatability for
236 positions further away from the vortex centre. Therefore, in table 3, the repeatability of surface
237 pressure measurements for the lowest swirl ratio is given for normalised radial locations of $r/D_3 \leq$
238 0.1 and larger than 0.1.
239
240 Table 3: Repetition uncertainties for velocity components (a) and surface pressures (b) in *M1*, *S1*, *S2*, *S3* and for $S =$
241 0.30 and $S = 0.69$

a)

| | $u_\theta/u_{ref}$ [-] | $u_r/u_{ref}$ [-] | $u_z/u_{ref}$ [-] | $u_\theta/u_{ref}$ [-] | $u_r/u_{ref}$ [-] | $u_z/u_{ref}$ [-] |
|---|---|---|---|---|---|---|
| | S = 0.30 | | | S = 0.69 | | |
| M1 | ±0.05 | ±0.06 | ±0.02 | ±0.04 | ±0.03 | ±0.01 |
| S1 | ±0.07 | ±0.06 | ±0.03 | ±0.02 | ±0.03 | ±0.02 |
| S2 | ±0.03 | ±0.10 | ±0.03 | ±0.05 | ±0.02 | ±0.02 |
| S3 | ±0.02 | ±0.05 | ±0.02 | ±0.04 | ±0.07 | ±0.02 |

b)

| | $p/p_{ref_{(r/D3 \leq 0.1)}}$ [-] | $p/p_{ref_{(r/D3 > 0.1)}}$ [-] | $p/p_{ref}$ [-] |
|---|---|---|---|
| | S = 0.30 | | S = 0.69 |
| M1 | ±0.31 | ±0.07 | ±0.12 |
| S1 | ±0.17 | ±0.07 | ±0.07 |
| S2 | ±0.49 | ±0.16 | ±0.11 |
| S3 | ±0.14 | ±0.06 | ±0.06 |

In what follows, the measurement repeatability is used to quantify the experimental uncertainty since statistical and device uncertainties are assumed to be reflected within the uncertainty given by the repeatability. Therefore, the repeatability is assumed to provide a reasonable estimate for the experimental uncertainties.

## 3. RESULTS

To assess the influence of the simulator's geometry and corresponding geometric changes, in this section, flow field and surface pressure data obtained in *M1*, *S1*, *S2*, and *S3* are compared. The very nature of the experimental equipment and the scale of the generator prevents in some cases a detailed knowledge of the flow structure across the entire flow field. As a result, for some simulations presented below, the complex flow structure inside the vortex could not be captured in detail. However, sufficient data has been gathered which we postulate enables a relative comparison of flow fields and as a result provides an insight into the question at hand, i.e., does the geometry of the simulator influence the generated tornado-like flow field?

### 3.1. SIMULATIONS IN S1 AND M1

#### 3.1.1. The flow fields

The 3-D mean velocity fields obtained in *S1* and *M1* for *S* = 0.30 and *S* = 0.69 are shown in figure 2.
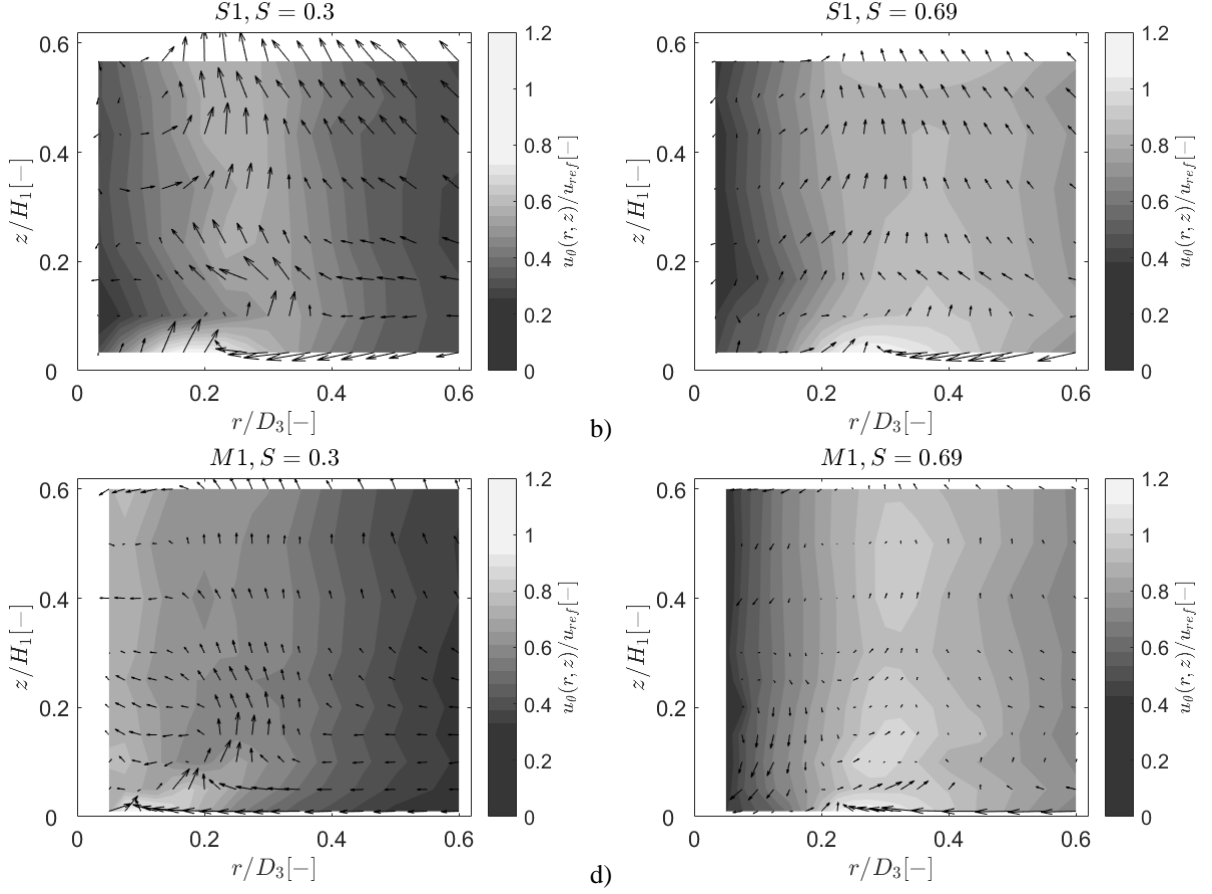
**Fig. 2** 3-D mean velocity fields in *S1* and *M1* for *S = 0.30* and *S = 0.69*. The normalised circumferential velocity component is shown as contour and the 2-D vector field indicates the vector based on the radial and vertical velocity component

Figure 2 highlights a number of similarities, e.g., for both swirl ratios in *S1* and *M1*, the circumferential velocity component increases towards the vortex core radius and reaches the overall maximum close to the surface. In *S1*, for the lower swirl ratio ($S = 0.30$) the core radius of the simulated vortex is approximately defined at $r/D_3 = 0.2$, whereas for the same swirl ratio in *M1*, the vortex core radius extends to about $r/D_3 = 0.1$. For the larger swirl ratio ($S = 0.69$) the core radius increases to a normalised radial distance equal to approximately $r/D_3 = 0.3$ in both simulators. Figure 2 also reveals a strong radial inflow close to the simulator's surface up to the position where the corresponding overall maximum of the circumferential velocity component occurs. This flow behaviour was found to be present for both swirl ratios in both simulators.

Figure 2a shows that for $S = 0.30$ in *S1*, radial inflow is dominant inside the vortex core (i.e., $r/D_3 \leq 0.2$) and for normalised heights $z/H_1 < 0.3$. This finding, in combination with the radial outflow from the vortex centre at larger normalised heights ($z/H_1 > 0.3$) could lead to the conclusion of a flow structure similar to what might be expected for a 'vortex breakdown'. For the larger swirl ratio, a central outflow is observed for all heights in *S1* (Figure 2b). This is a flow behaviour similar to what is expected in a two-celled vortex structure.

The 3-D velocity field obtained in the medium simulator (*M1*) for $S = 0.30$ shows tentative evidence

292  to suggest the presence of a counter-clockwise rotating cell near the surface close to the vortex
293  centre covering a normalised area of approximately 0.1 x 0.1(Figure 2c). At greater heights, the
294  vortex core is dominated by radial inflow and updraft, which turns into a downdraft at a normalised
295  height of $z/H_1 = 0.6$, potentially suggesting a second counter-clockwise rotating cell in the vortex
296  core at greater heights. With increasing swirl ratio ($S = 0.69$) in $M1$, a downdraft is detected in the
297  vortex centre, which seems to feed into the radial outflow observed at the lowest height (Figure
298  2d). This describes a flow structure, which might be expected for a two-celled vortex. However,
299  the central downdraft is directed slightly towards the simulator's centre, which in general is not
300  expected in a 'typical' two-celled vortex; however, was also observed by Haan et al. [18] for a high
301  swirl ratio.

302
303
304  **3.1.2. The effect of the simulator's geometry on the flow field ($T1$)**
305
306  In order to allow a representative comparison between flow fields simulated in $S1$ and $M1$, flow
307  characteristics at equal relative heights ($z/H_1$) are compared in this section. Table 4 illustrates that
308  for each comparison two heights are determined ($z_1$ and $z_2$) which lead to the same relative heights
309  in simulator $S1$ and $M1$.

310
311  Figure 3 illustrates the radial profile of circumferential (a), radial (b) and vertical (c) velocity
312  components obtained in $S1$ and $M1$ for $S = 0.30$ (1) and $S = 0.69$ (2) at corresponding relative
313  heights given in table 4.

314
315  Table 4: Absolute ($z$) and relative ($z/H_1$) heights for the comparison of flow fields simulated $S1$ and $M1$ for $S = 0.30$
316  and $S = 0.69$

|  | S1 | M1 |
|---|---|---|
| $z_1$ [m] | 0.03 | 0.10 |
| $z_2$ [m] | 0.15 | 0.50 |
| $z_1/H_1$ | 0.1 | 0.1 |
| $z_2/H_1$ | 0.5 | 0.5 |

317



318  a1)                                                                a2)
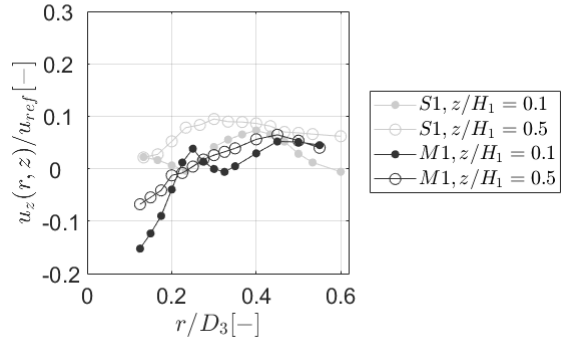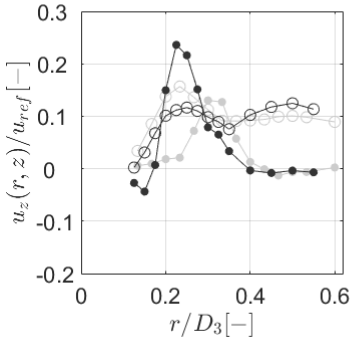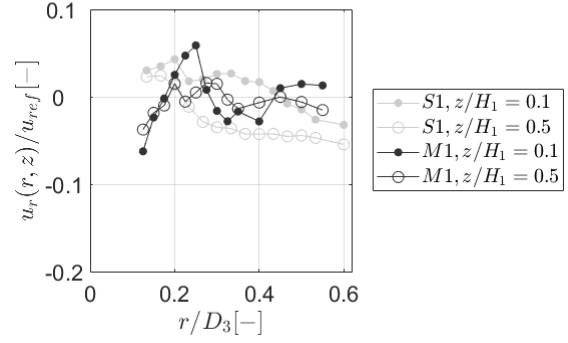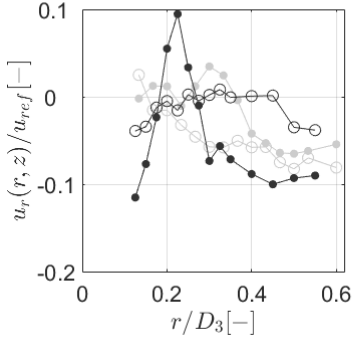
319 b1)
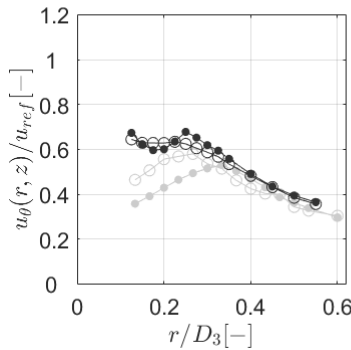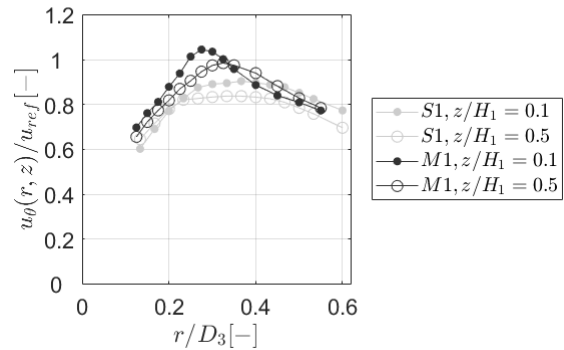


320 c1)
321
322 **Fig. 3** Radial profile of mean circumferential (a), radial (b) and vertical (c) velocity components obtained in *S1* and
323 *M1* for $S = 0.30$ (1) and $S = 0.69$ (2) at corresponding relative heights ($z/H_1$)
324

325 Figure 3 shows differences larger than the corresponding experimental uncertainty (defined in table
326 3) between the flow fields obtained in *S1* and *M1* for both swirl ratios. In what follows, differences
327 between velocity components obtained in different simulators will be presented in the following
328 form: ($\delta u_x = \left| (u_x(r,z)/u_{ref})_{S1} - (u_x(r,z)/u_{ref})_{M1} \right|$).
329

330 Circumferential velocity components obtained in *S1* and *M1* for the smaller swirl ratio ($S = 0.30$)
331 differ significantly at radial distances $< 0.3$ $r/D_3$ for both heights investigated (Figure 3a1). In this
332 flow region, circumferential velocity components were found to be larger by approximately $0.2\delta u_\theta$
333 in *M1* compared to *S1*. Figure 3b1 reveals differences between the radial profile of radial velocity
334 components in *S1* and *M1*. For the lowest height investigated, differences of approximately $0.1\delta u_r$
335 can be observed. Those differences originate from the radial inflow, which extends further in *M1*
336 compared to *S1*. At the larger relative height ($z/H_1 = 0.5$) and at a radial distance of $r/D_3 = 0.1$, a
337 weak central outflow can be detected in *S1*, whereas radial inflow seems to dominate the flow field
338 in *M1*. Vertical velocity components obtained in *M1* for $S = 0.30$ differ only at the lower height
339 investigated (Figure 3c1). At this height ($z/H_1 = 0.1$) and at a radial distance of $r/D_3 = 0.2$, vertical
340 velocities are found to be larger by $0.2\delta u_z$ in *M1* compared to *S1*. This is the case because the
341 maximum vertical updraft occurs at smaller radial distances in *M1* compared to *S1*.
342

343    For $S = 0.69$, circumferential velocity components reveal differences of up to $0.2\delta u_\theta$ at a flow
344    region around the vortex core ($0.2 < r/D_3 < 0.4$) for both heights investigated (Figure 3a2). The
345    region of maximum circumferential velocities is not as well defined in *S1* compared to *M1*, which
346    leads to a relatively uniform distribution of circumferential velocities around the vortex core in *S1*.
347    Differences observed between radial velocities in *S1* and *M1* are small and therefore, are largely
348    masked by the experimental uncertainty (Figure3b2). Only at the lowest height investigated ($z/H_1$
349    $= 0.1$), the weak radial inflow present in *M1* and the weak radial outflow observed in *S1* causes
350    differences larger than the measurement uncertainty of approximately $0.1\delta u_r$. Largest differences
351    between vertical velocity components in *S1* and *M1* are obtained at radial distances $< 0.2r/D_3$ for
352    both heights investigated (Figure 3c2). In this region, the flow field at the lowest height ($z/H_1 =$
353    $0.1$) differs by about $0.15\delta u_z$, whereas differences in the larger height are $0.05\delta u_z$. Observed
354    differences can be explained by the downdraft captured in *M1* which extends to approximately $r/D_3$
355    $= 0.2$, whereas in *S1* the downdraft occurs at radial distances closer to the simulator's centre.
356
357    When highlighting those differences between flow fields simulated in different simulators but
358    aspect ratio and swirl ratio parity, the question arises, whether, the swirl ratio defined based on the
359    guide vane angle (Eq. 6) might not be a representative parameter to determine the similarity of flow
360    characteristics. In order to address this question in more detail the following section analyses swirl
361    ratios defined at different locations in the generated flow fields.
362
363    **3.1.3. The swirl ratio of flow fields simulated in *S1* and *M1***
364
365    In this section, swirl ratios are calculated for the flow fields simulated in *S1* and *M1* using the
366    following equations:
367

$$S_2 = \frac{\Gamma_{average\ (r=D_3/2)}\ D_3}{4Q} \tag{7}$$

368

$$with\ \Gamma_{average\ (r=D_3/2)} = \frac{1}{N}\sum_{i=1}^{N} (\Gamma_{(r=D_3/2)})_i$$

369
370

$$S_3 = \frac{\Gamma_{(R)}\ D_3}{4Q} \tag{8}$$

371
372

$$S_4 = \frac{\Gamma_{(R)}\ R}{2Q} \tag{9}$$

373
374
375    Here, $\Gamma(r)$ is the circulation ($\Gamma(r) = 2\pi r u_\theta(r)$), $N$ is the number of measurement heights in the
376    corresponding simulator and $i$ represents an individual measurement height.
377
378    The definition adopted in equation (7) is based on the height average of swirl ratios at $r = D_3/2$ and
379    is identical to the swirl ratio used by Tang et al. [24]. Equation (8) is similar to the definition
380    adopted by Refan and Hangan [22], whereas Haan et al. [18] introduced equation (9).
381
382    The difference between the definitions shown in equations (6 and 7) and equation (8) is that the
383    length scale in the numerator of $S_3$ (Eq. 8) is not identical to the radial distance at which the
384    circulation is estimated. Furthermore, it needs to be mentioned that the swirl ratio defined in
385    equation (6) is the only swirl ratio (from those presented) that is independent from any direct

386 velocity measurement and that swirl ratios defined by equations (7 – 9) are calculated based on
387 parameters (such as $\Gamma$ and $R$) which are dependent on parameters defined in equations (1 – 6).
388
389 An overview of corresponding swirl ratio values for the flow fields obtained in $S1$ and $M1$ is
390 presented in table 5.
391
392 Table 5: Swirl ratios ($S$ and $S_2 – S_4$) defined at different locations in the flow fields of $M1$ and $S1$

a)

| | Figure | S | $S_2$ | $S_3$ | $S_4$ |
|---|---|---|---|---|---|
| S1 | 2a | 0.30 | 0.35 | 0.30 | 0.11 |
| M1 | 2c | 0.30 | 0.38 | 0.28 | 0.03 |

393

b)

| | Figure | S | $S_2$ | $S_3$ | $S_4$ |
|---|---|---|---|---|---|
| S1 | 2b | 0.69 | 0.81 | 0.62 | 0.35 |
| M1 | 2d | 0.69 | 0.82 | 0.55 | 0.25 |

394
395 Because of the forced aspect ratio and guide vane angle parity between both simulators, $S$ is
396 identical (Table 5a and 5b).
397
398 Table 5 illustrates that for both flow fields in both simulators, $S_4$ shows the lowest and $S_2$ the highest
399 swirl ratio. The reason for this can be found in the numerators of equations (9 and 7). Since the
400 circulation is proportional to the radial distance, $S_2$ and $S_4$ are proportional to the square of the
401 radial distance. Consequently, $S_4$ is calculated at relatively small radial distances ($r = R$) and $S_2$ is
402 calculated at relatively large radial distances ($r = D_3/2$). Since, $S_3$ is defined based on a combination
403 of $R$ and $D_3/2$ (Eq. 8) its value lies in-between the values obtained for $S_2$ and $S_4$ (Table 5).
404
405 In order to determine whether swirl ratio parity between flow fields simulated in $S1$ and $M1$ is
406 given regardless of the adapted definition, the accuracy with which each swirl ratio can be
407 determined needs to be quantified. For $S$ (Eq. 6), a possible source of uncertainty is the accuracy
408 with which the guide vane angle can be adjusted. For $S_2$ and $S_3$, the uncertainty is partly determined
409 by the uncertainty of the circumferential velocity component. For $S_4$ the uncertainty of $R$ is an
410 additional limitation for the swirl ratio's accuracy. As a result of those uncertainties, the swirl ratios
411 presented in equations (6 – 8) are only accurate to one decimal place. The accuracy of the swirl
412 ratio defined in equation (9) is even lower. With this additional information, table 5 reveals that
413 swirl ratio parity is given for both flow fields investigated in $S1$ and $M1$, regardless of which
414 definition for the swirl ratio is used. This finding suggests that the geometric differences of both
415 simulators are the cause of observed differences between the flow fields.
416
417 Additionally, it is noted that swirl ratios presented here are calculated based on time-averaged
418 quantities of the circulation and the flow rate and therefore, conclusions can only be drawn with
419 respect to the time-averaged flow behaviour. The instantaneous flow field of two vortices of similar
420 swirl ratio may differ significantly. Furthermore, all swirl ratio definitions presented in this section
421 focus on the similarity between circumferential velocity components. Therefore, no conclusion can
422 be drawn regarding the similarity of radial and vertical velocity components.

**3.1.4. The effect of the simulator's geometry on the surface pressure field (*T1*)**

Figures 4 illustrates surface pressure distributions that arise as a result of the two flow fields investigated in *S1* and *M1* for *S* = 0.30 and *S* = 0.69, respectively. In general, it can be observed that surface pressure distributions obtained for *S* = 0.30 (Figure 4a) increase at a faster rate from the vortex centre towards larger radial distances compared to *S* = 0.69 (Figure 4b). Despite the suggested central downdraft for *S* = 0.69 in *S1* and *M1*, the surface pressure distribution of the corresponding vortex does not show the expected two-celled vortex structure near the simulator's centre. A potential reason for this could be that the effect of the downdraft on surface pressure measurements is too small to be captured compared to the effect of the circumferential velocity component.

Figure 4a highlights that despite of the observed flow field differences between vortices simulated in *S1* and *M1* for *S* = 0.30, surface pressure distributions are in good agreement and small differences lie within the experimental uncertainty. The same applies for surface pressure distributions of the larger swirl ratio for radial distances > $|0.2r/D_3|$ (Figure 4b). However, around the vortex centre, a pressure deficit which is smaller by about $0.5\delta p$ is observed in *M1* compared to *S1* ($\delta p = \left| (p(r,z=0)/p_{ref})_{S1} - (p(r,z=0)/p_{ref})_{M1} \right|$).
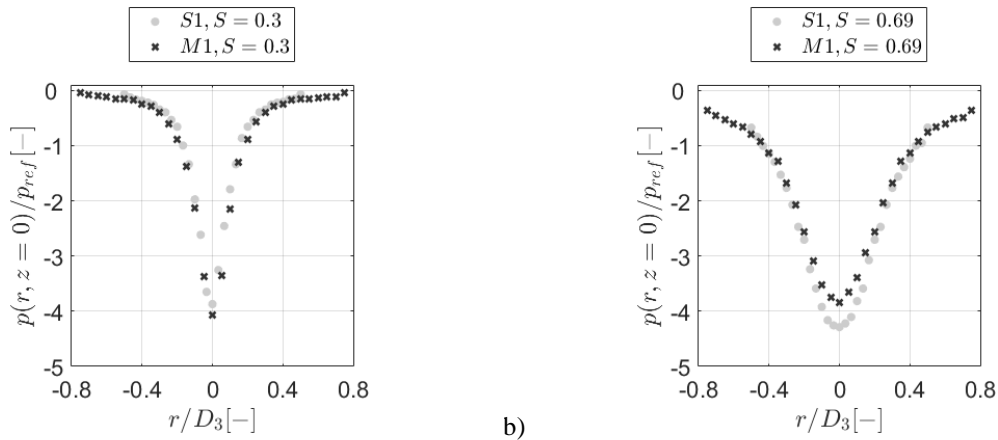


a)                                                                                  b)

**Fig. 4** Mean surface pressure distributions measured in *S1* and *M1* for *S* = 0.30 (a) and *S* = 0.69 (b)

**3.2. SIMULATIONS IN S1, S2 AND S3**

**3.2.1 The effect of the convection chamber height on the flow field (*T2*)**

In this section, the effect of changing the convection chamber height ($H_2$) in the small generator (whilst keeping other geometric parameters and the swirl ratio defined in equation (6) constant) is investigated.
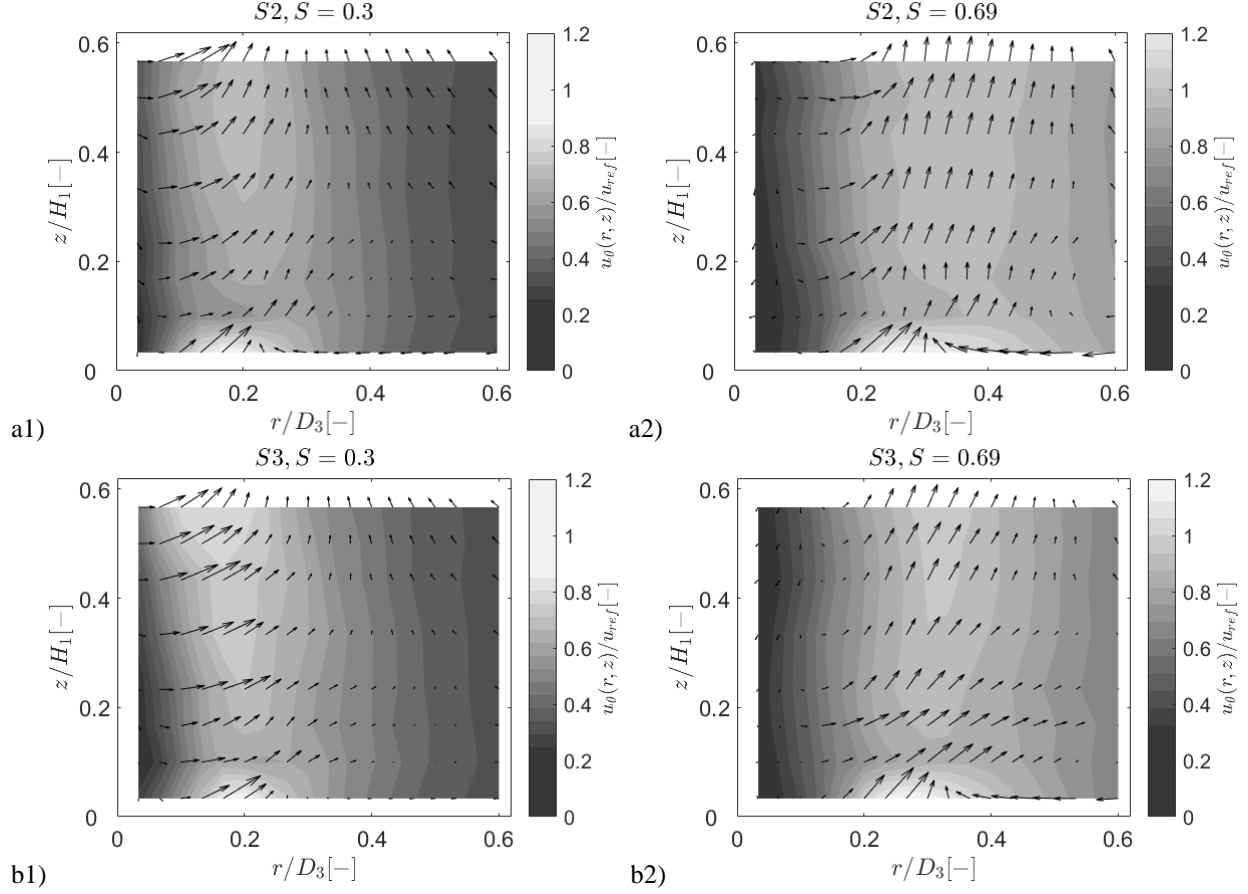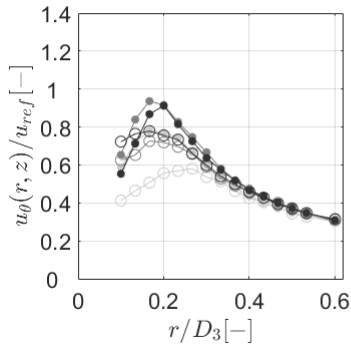
**Fig. 5** Mean 3-D velocity fields in *S2* and *S3* for *S* = 0.30 and *S* = 0.69. The normalised circumferential velocity component is shown as contour and the 2-D vector field indicates the vector based on the radial and vertical velocity component.

The 3-D velocity fields obtained in *S2* (where the convection chamber height is reduced by ~38%) and *S3* (where the convection chamber height is reduced by ~75%) for both swirl ratios are shown in figure 5. Also, for those simulations a number of similarities can be highlighted. For all simulations conducted in *S2* and *S3*, radial outflow dominates the vortex core, which feeds into an updraft at a radial distance approximately equal to the corresponding vortex core. This flow behaviour appears to become more distinct with decreasing $H_2$, irrespective of the swirl ratio. In both simulators (*S2* and *S3*) for the lower swirl ratio (*S* = 0.30) the core radius is approximately defined at $r/D_3$ = 0.2. For the larger swirl ratio (*S* = 0.69) the vortex core size increases to a normalised radial distance equal to approximately $r/D_3$ = 0.3 (Figure 5a2 and 5b2). Furthermore, the relatively strong radial inflow close to the surface up to the position where the overall circumferential velocity maximum occurs (shown in figure 2a and 2b) appears to weaken with decreasing $H_2$ (Figure 5). For *S* = 0.30, the strong radial outflow and updraft observed in the vortex core of *S2* and *S3* suggests that the downdraft in *S1*, which seems to terminate aloft a stagnation point at a normalised height of approximately $z/H_1$ = 0.3 (Figure 2a), lowers and reaches the surface of simulator *S2* and *S3* (Figure 5a and 5c). The overall flow structure for all simulations for the larger swirl ratio suggests a vortex structure similar to what might be expected in a two-celled vortex (Figure 2b, 5b and 5d). The radial outflow inside the vortex core obtained in *S1*, *S2* and *S3* suggests a central downdraft.
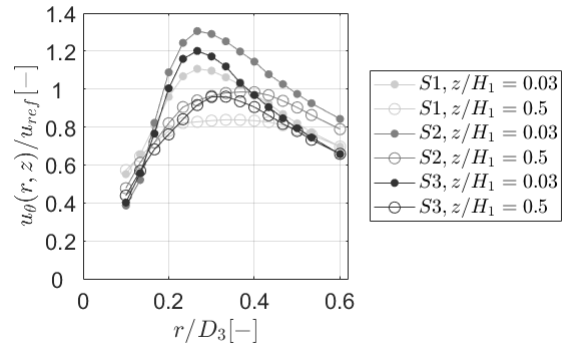
481
482 For more details, differences between circumferential, radial and vertical velocity components at
483 equal relative heights ($z/H_1$) in the simulators are shown in figure 6. Table 6 provides an overview
484 of heights investigated.

485
486 Table 6: Absolute ($z$) and relative ($z/H_1$) heights for the comparison of flow fields simulated $S1$, $S2$ and $S3$ for $S =$
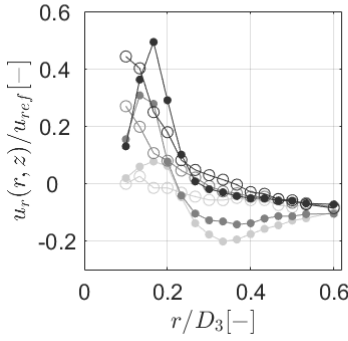487 0.30 and $S = 0.69$

|  | S1 | S2 | S3 |
|---|---|---|---|
| $z_1$ [m] | 0.01 | 0.01 | 0.01 |
| $z_2$ [m] | 0.15 | 0.15 | 0.15 |
| $z_1/H_1$ | 0.03 | 0.03 | 0.03 |
| $z_2/H_1$ | 0.50 | 0.50 | 0.50 |

488



489   a1)                                                                        a2)

490    b1)                                                b2)
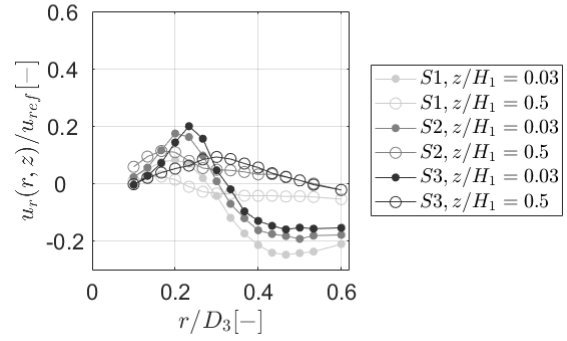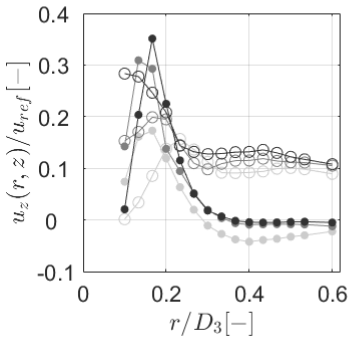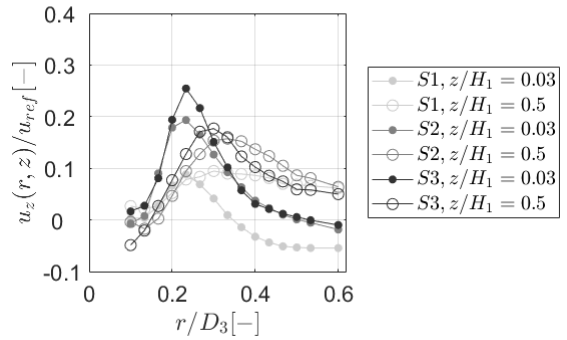


491    c1)                                                c2)

**Fig. 6** Radial profile of circumferential (a), radial (b) and vertical (c) velocity components obtained in *S1*, *S2* and *S3*
for $S = 0.30$ (1) and $S = 0.69$ (2) at the corresponding relative heights ($z/H_1$)

Figure 6a1 illustrates that circumferential velocity components obtained for $S = 0.30$ differ
significantly at radial distances $< 0.2$ $r/D_3$ (Figure 6a1). Differences of about $0.3\delta u_\theta$ can be
observed between vortices simulated in *S1* and *S3* at $z/H_1 = 0.5$. For S = 0.69 (Figure 6a2), the
radial profiles of circumferential velocity components reveal differences of up to $0.2\delta u_\theta$ and
$0.1\delta u_\theta$ around the region of maximum circumferential velocities for $z/H_1 = 0.5$ and $z/H_1 = 0.03$,
respectively.

Differences larger than the experimental uncertainty are also found for radial velocity components
(Figures 6b1 and 6b2). For S = 0.30, the radial outflow at radial distances $< 0.2$ $r/D_3$ increases
significantly with decreasing $H_2$ (Figure 6b1). Differences of up to $0.3\delta u_r$ are found when
comparing *S1* with *S2*, and a comparison between *S1* with *S3* reveals differences of approximately
$0.4\delta u_r$. In addition, at $r/D_3 = 0.3$, a decrease in radial inflow can be observed with decreasing $H_2$
at the lower height ($z/H_1 = 0.03$). For the larger swirl ratio (S = 0.69, Figure 6b2), a reduction of
$H_2$ by 75% seems to cause differences of about $0.2\delta u_r$. Although, differences between the flow
fields of the lower swirl ratio seem to be more distinct, a similar trend can perhaps be inferred for
radial velocity components of the larger swirl ratio.

Figures 6c1 and 6c2 illustrate that the vertical updraft around the corresponding vortex core region
intensifies with decreasing $H_2$ for both swirl ratios. For the lower swirl ratio (S = 0.30), this causes

515  differences of up to $0.15\delta u_z$ between *S1* and *S2,* and up to $0.3\delta u_z$ between *S1* and *S3* at $z/H_1 = 0.5$
516  and $r/D_3 = 0.1$ (Figures 6c1). For the larger swirl ratio, differences are more distinct at the lower
517  height (Figure 6c2). In this case, differences of about $0.1\delta u_z$ and $0.15\delta u_z$ are found when
518  comparing results obtained at $r/D_3 = 0.25$ in *S1* to *S2* and *S3*, respectively.
519
520  **3.2.2 The effect of the convection chamber height on the surface pressure field (*T2*)**
521
522  The radial profiles of surface pressures measured in *S1*, *S2* and *S3* for $S = 0.30$ (a) and $S = 0.69$ (b)
523  are presented in figure 7. Figure 7 reveals that despite of flow field differences highlighted for S =
524  0.30, the surface pressure distributions illustrated in figure 7a seem to be largely unaffected by the
525  changes of $H_2$. The surface pressure distribution of the larger swirl ratio on the other hand (Figure
526  7b) shows significant differences for most radial distances. In particular around the vortex centre,
527  differences of about $1.5\delta p$ are illustrated between surface pressure distributions measured in *S2* and
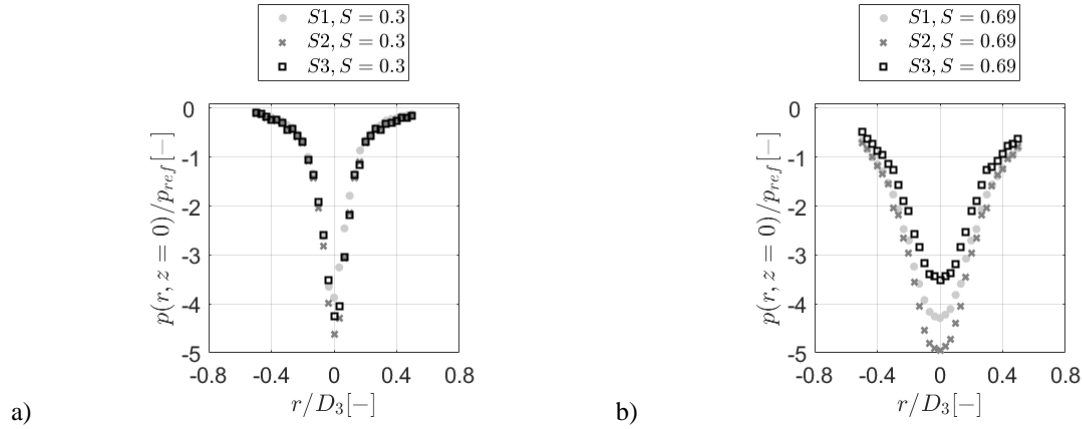528  *S3*.



529  a)  b)
530
531        **Fig. 7** Mean surface pressure distributions obtained in *S1*, *S2* and *S3* for $S = 0.30$ (a) and $S = 0.69$ (b)
532
533  **4. CONCLUDING REMARKS**
534
535  Based on this analysis, the following main conclusions can be drawn:
536
537  • Time averaged velocity and surface pressure data have been presented and illustrate (in
538    keeping with previous work) that the swirl ratio has an effect on the vortex size, pressure
539    distribution and velocity characteristics.
540
541  • Velocity and surface pressure characteristics of vortices generated in simulators of different
542    geometry and scale, but with swirl ratio and aspect ratio parity can differ significantly.
543    Based on this, it is suggested that ensuring aspect ratio and swirl ratio parity between
544    different simulators is not sufficient to generate similar vortices with similar velocity and
545    surface pressure characteristics, i.e. not surprisingly, all boundary conditions govern the
546    flow.
547
548  • Flow field and surface pressure characteristics of tornado-like vortices appear also to be a
549    function of the convection chamber height.
550

- It was found that the effect of the simulator's geometry on the flow and surface pressure field can be swirl ratio dependent.

- It has been shown that an agreement between surface pressure distributions is not sufficient to conclude flow field similarity.

**Compliance with Ethical Standards**

Conflict of Interest: The authors declare that they have no conflict of interest.

**REFERENCES**

1. *Solari G, Rainisio D and De Gaetano P (2017) Hybrid simulation of thunderstorm outflows and wind-excited response of structures. Meccanica 52:3197-3220. https://doi.org/10.1007/s11012-017-0718-x*

2. *Brusco S, Lerzo V and Solari G (2019) Directional response of structures to thunderstorm outflows. Meccanica:1-26. https://doi.org/10.1007/s11012-019-00986-5.*

3. *Jesson M, Lombardo FT, Sterling M, Baker CJ (2019) The physical simulation of a transient, downburst-like event – How complex does it need to be? Journal of Wind Engineering and Industrial Aerodynamics 189:135-150. https://doi.org/10.1016/j.jweia.2019.03.021*

4. *Letchford CW, Mans C, Chay MT (2002) Thunderstorms–their importance in windengineering (a case for the next generation wind tunnel). Journal of Wind Engineering and Industrial Aerodynamics 90:1415–1433. https://doi.org/10.1016/S0167-6105(02)00262-3*

5. *NOAA 2011 National Oceanic and Atmospheric Administration – U.S. Department of Commerce. https://www.ncdc.noaa.gov/sotc/tornadoes/201113. Accessed: 6 June 2018.*

6. *Hoecker WH (1960) Wind speed and air flow patterns in the Dallas tornado of April 2, 1957. Monthly Weather Review 88:167-180. https://doi.org/10.1175/1520-0493(1960)088<0167:WSAAFP>2.0.CO;2*

7. *Winn WP, Hunyady SJ, Aulich GD (1999) Pressure at the ground in a large tornado. Journal of Geophysical Research: Atmospheres 104:22067-22082. https://doi.org/10.1029/1999JD900387*

8. *Wurman J, Gill S (2000) Finescale Radar Observations of the Dimmitt, Texas (2 June 1995), Tornado. Monthly Weather Review 128:2135-2164. https://doi.org/10.1175/1520-0493(2000)128<2135:FROOTD>2.0.CO;2*

9. *Lee J, Samaras T, Young CR (2004) Pressure measurements at the ground in an F-4 tornado. The 22nd Conference on Severe Local Storms, Anonymous Hyannis, MA.*

10. *Wurman J and Alexander CR (2004) The 30 May 1998 Spencer, South Dakota, Storm. Part II: Comparison of Observed Damage and Radar-Derived Winds in the Tornadoes. Monthly Weather Review 133:97-119.https://doi.org/10.1175/MWR-2856.1*

11. *Lee WC and Wurman J (2005) Diagnosed Three-Dimensional Axisymmetric Structure of the Mulhall Tornado on 3 May 1999. Journal of the Atmospheric Sciences 62:2373-2393. https://doi.org/10.1175/JAS3489.1*

12. *Karstens CD, Samaras TM, Lee BD, Gallus Jr WA, Finley CA (2010) Near-Ground Pressure and Wind Measurements in Tornadoes. Monthly Weather Review 138:2570-2588. https://doi.org/10.1175/2010MWR3201.1*

13. *Kosiba K, Wurman J (2010) The Three-Dimensional Axisymmetric Wind Field Structure of the Spencer, South Dakota, 1998 Tornado. Journal of the Atmospheric Sciences 67:3074-3083. https://doi.org/10.1175/2010JAS3416.1*

14. *Wurman J, Kosiba K, Robinson P (2013) In Situ, Doppler Radar, and Video Observations of the Interior Structure of a Tornado and the Wind–Damage Relationship. Bulletin of the American Meteorological Society 94:835-846. https://doi.org/10.1175/BAMS-D-12-00114.1*

15. *Refan M, Hangan H, Wurman J, Kosiba K (2017) Doppler radar-derived wind field of five tornado events with application to engineering simulations. Engineering Structures 148:509-521. https://doi.org/10.1016/j.engstruct.2017.06.068*

16. *Ward NB, (1972) The Exploration of Certain Features of Tornado Dynamics Using a Laboratory Model. Journal of the Atmospheric Sciences 29:1194-1204. https://doi.org/10.1175/1520-0469(1972)029<1194:TEOCFO>2.0.CO;2*

17. *Church CR, Snow JT, Baker GL, Agee EM (1979) Characteristics of Tornado-Like Vortices as a Function of Swirl Ratio: A Laboratory Investigation. Journal of the Atmospheric Sciences 36:1755-1776. https://doi.org/10.1175/1520-0469(1979)036<1755:COTLVA>2.0.CO;2*

18. *Haan Jr FL, Sarkar PP, Gallus WA (2008) Design, construction and performance of a large tornado simulator for wind engineering applications. Engineering Structures 30:1146-1159. https://doi.org/10.1016/j.engstruct.2007.07.010*

19. *Mishra AR, James DL, Letchford CW (2008) Physical simulation of a single-celled tornado-like vortex, Part A: Flow field characterization. Journal of Wind Engineering and Industrial Aerodynamics 96:1243-1257. https://doi.org/10.1016/j.jweia.2008.02.063*

20. *Sabareesh GR, Matsui M, Tamura Y (2012) Dependence of surface pressures on a cubic building in tornado like flow on building location and ground roughness. Journal of Wind Engineering and Industrial Aerodynamics 103:50-59. https://doi.org/10.1016/j.jweia.2012.02.011*

21. *Refan M, Hangan H (2016) Characterization of tornado-like flow fields in a new model scale wind testing chamber. Journal of Wind Engineering and Industrial Aerodynamics 151:107-121. https://doi.org/10.1016/j.jweia.2016.02.002*

22. *Refan M and Hangan H (2018) Near surface experimental exploration of tornado vortices. Journal of Wind Engineering & Industrial Aerodynamics 175:120–135. https://doi.org/10.1016/j.jweia.2018.01.042*

633   23. *Gillmeier S, Sterling M, Hemida H, Baker CJ (2018) A reflection on analytical tornado-like*
634       *vortex flow field models. Journal of Wind Engineering and Industrial Aerodynamics 174:10-*
635       *27. https://doi.org/10.1016/j.jweia.2017.12.017*

636   24. *Tang Z, Feng C, Wu L, Zuo D, James DL (2018a) Characteristics of Tornado-Like Vortices*
637       *Simulated in a Large-Scale Ward-Type Simulator. Boundary-Layer Meteorology 166:327–*
638       *350. http://dx.doi.org/10.1007/s10546-017-0305-7*

639   25. *Davies-Jones RP (1973) The Dependence of Core Radius on Swirl Ratio in a Tornado*
640       *Simulator. Journal of the Atmospheric Sciences 30:1427-1430.*
641       *https://doi.org/10.1175/1520-0469(1973)030<1427:TDOCRO>2.0.CO;2*

642   26. *Tang Z, Zuo D, James D, Eguchi Y, Hattori Y (2018b) Effects of Aspect Ratio on Laboratory*
643       *Simulation of Tornado-Like Vortices. Wind and Structures 27:111-121.*
644       *http://dx.doi.org/10.12989/was.2018.27.2.111*

645   27. *Wan CA and Chang CC (1972) Measurement of the Velocity Field in a Simulated Tornado-*
646       *Like Vortex Using a Three-Dimensional Velocity Probe. Journal of the Atmospheric*
647       *Sciences 29:116-127. https://doi.org/10.1175/1520-*
648       *0469(1972)029<0116:MOTVFI>2.0.CO;2*

649   28. *Jischke MC and Parang M (1974) Properties of Simulated Tornado-Like Vortices. Journal*
650       *of the Atmospheric Science 11:506–512. https://doi.org/10.1175/1520-*
651       *0469(1974)031%3C0506:POSTLV%3E2.0.CO;2*

652   29. *Zhang W and Sarkar PP (2012) Near-ground tornado-like vortex structure resolved by*
653       *particle image velocimetry (PIV). Exp. Fluids 52:479-493. https://doi.org/10.1007/s00348-*
654       *011-1229-5*

655   30. *Hashemi-Tari P, Gurka R, Hangan H (2010) Experimental investigation of tornado-like*
656       *vortex dynamics with swirl ratio: The mean and turbulent flow fields. Journal of Wind*
657       *Engineering and Industrial Aerodynamics 98:936-944.*
658       *https://doi.org/10.1016/j.jweia.2010.10.001*

659   31. *Gillmeier S., Sterling, M., Baker, C., 2017. An analysis of non-stationary processes in*
660       *tornado-like vortices. International Workshop on Physical Modelling of Flow and*
661       *Dispersion Phenomena. France*

662   32. *Church CR, Snow JT, Agee, EM (1977) Tornado Vortex Simulation at Purdue University.*
663       *American Metrological Society 58:900–908. https://doi.org/10.1175/1520-*
664       *0477(1977)058<0900:TVSAPU>2.0.CO;2*